Heterogeneous Catalysis of Lanthanoid Ions for the Hydrolysis of p-Nitrophenyl Phosphate Enhanced by Incorporation to Cyano-Bridged Heterometallic Coordination Polymers

Heterogeneous Catalysis of Lanthanoid Ions for the Hydrolysis of *p*-Nitrophenyl Phosphate Enhanced by Incorporation to Cyano-Bridged Heterometallic Coordination Polymers

Hiroyasu Tabe, Shoma Yorozu, Yusuke Yamada

Tabe, H., Yorozu, S., & Yamada, Y. (2022). Heterogeneous Catalysis of Lanthanoid Ions for the Hydrolysis of p-Nitrophenyl Phosphate Enhanced by Incorporation to Cyano-Bridged Heterometallic Coordination Polymers. *The Journal of Physical Chemistry C*. 126, 4365–4373. https://doi.org/10.1021/acs.jpcc.1c10369

Heterogeneous Catalysis of Lanthanoid Ions for the Hydrolysis of *p*-Nitrophenyl Phosphate Enhanced by Incorporation to Cyano-bridged Heterometallic Coordination Polymers

Hiroyasu Tabe[a], Shoma Yorozu[b], and Yusuke Yamada[bc]*

[a]Institute for Integrated Cell-Material Sciences (iCeMS), Institute for Advanced Study (IAS), Kyoto University, Yoshida-Hommachi, Sakyo-ku, Kyoto 606-8501, Japan.

[b]Department of Applied Chemistry and Bioengineering, Graduate School of Engineering, Osaka City University, 3-3-138 Sugimoto, Sumiyoshi-ku, Osaka 558-8585, Japan.

[c]Research Center for Artificial Photosynthesis (ReCAP), Osaka City University, 3-3-138 Sugimoto, Sumiyoshi-ku, Osaka 558-8585, Japan.

*E-mail: ymd@osaka-cu.ac.jp.

ABSTRACT

Solid materials containing a lanthanoid ion (Ln^{III}, Ln = Tb or Eu), i.e., lanthanoid oxide ($Ln^{III}_2O_3$), lanthanoid ions immobilized on silica-alumina by cation exchange (Ln^{III}/Al-SiO$_2$) and lanthanoid ions incorporated into cyano-bridged heterometallic coordination polymers ($[Ln^{III}(H_2O)_x]_y[M^C(CN)_6]$, Ln = Tb or Eu; M^C = Fe^{III} or Ru^{II}; $x \geq 2$), were examined as heterogeneous catalysts for hydrolysis of p-nitrophenyl phosphate (p-NPP). $Ln^{III}_2O_3$ and Ln^{III}/Al-SiO$_2$ exhibit lower catalytic activity (~50% and ~55% for 72 h, respectively) than Ln^{III} ions used as homogeneous catalysts (~65%) for the hydrolysis of p-NPP. Ex-situ IR measurements after the hydrolysis of p-NPP indicated that active sites of the heterogeneous catalysts were inhibited by a product of dihydrogen phosphate. On the other hand, $[Ln^{III}(H_2O)_x]_y[M^C(CN)_6]$ exhibited higher activity ($\geq$80%) for the hydrolysis of p-NPP compared with not only the homogeneous Ln^{III} catalysts but also cyano-bridged heterometallic coordination polymers containing 3d-metal ions such as Fe^{III} ion (38%) previously reported as active catalysts. The high activity of $[Ln^{III}(H_2O)_x]_y[M^C(CN)_6]$ resulted from suitable interaction among Ln^{III} ions in the coordination polymers, p-NPP and water as evidenced by the ex-situ IR measurements.

INTRODUCTION

Organophosphates are a diverse group of pesticides and insecticides.[1−4] Residual organophosphates found in soils, irrigation, and air should be removed to prevent adverse effects on human health.[5−14] The residual organophosphates are usually removed by suitable adsorbents such as activated carbon. However, organophosphates at high concentrations cannot be removed entirely due to the limited capacity of the adsorbents.

Organophosphates at high concentrations can be efficiently degraded by catalytic materials.[15−18] In nature, a series of enzymes such as phosphatase and phosphodiesterase are used as catalysts for the hydrolytic decomposition of organophosphates.[19−22] Many enzymes hold metal ions at active sites. In this context, metal ions such as zinc, copper, cobalt, and mercury ions have been used as homogeneous catalysts for the hydrolysis of organophosphates.[23−30] Lanthanoid (Ln) ions are also available as the hydrolysis catalysts due to their strong Lewis acidity in aqueous solutions.[31−34] Recently, the higher catalytic activity of cerium(IV) ions than 3d-metal ions has been reported for organophosphates hydrolysis because 4f orbitals of Ce ion readily interact with the orbitals of the phosphate group in an organophosphate.[35−37]

Some metal ions have been reported to act as homogeneous catalysts highly active for the hydrolytic reaction in an aqueous solution. Heterogenization of the metal ions is strongly demanded for easy handling, high robustness, and facile separation after the catalytic reactions. However, the heterogenization often results in reducing the catalytic activity due to the limited diffusion of substrates and specific adsorption of products on the catalyst surfaces.

Herein, heterogenization of Ln^{III} catalysts is investigated for the catalytic hydrolysis of *p*-nitrophenyl phosphate (*p*-NPP, Figure 1) while maintaining their high catalytic activity. The
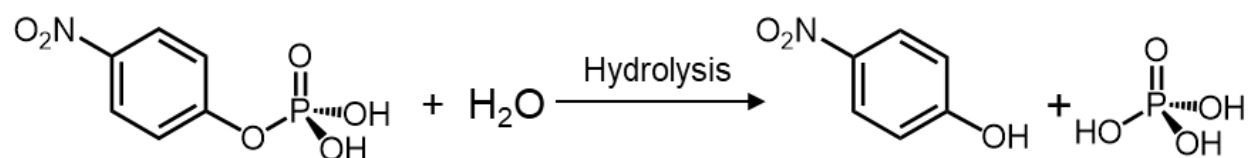
Figure 1. The chemical equation of the hydrolysis of *p*-nitrophenyl phosphate (*p*-NPP).

heterogenization of Ln^{III}-ion catalysts can be realized by three methods, *i.e.*, preparation of lanthanoid oxides ($Ln^{III}_2O_3$), immobilization of the Ln^{III} ions on silica-alumina (Al-SiO$_2$) by the cation-exchange reaction (Ln^{III}/Al-SiO$_2$), and syntheses of cyano-bridged heterometallic

coordination polymers containing Ln^{III} ions. Active sites of $Ln^{III}_2O_3$ are open Ln^{III} sites accidentally formed on their surfaces. Active sites of $Ln^{III}/Al-SiO_2$ are formed on Ln^{III} ions by the liberation of coordination water molecules. The catalytic/adsorption properties of open Ln^{III} ions are hardly tunable in $Ln^{III}_2O_3$ and $Ln^{III}/Al-SiO_2$. On the other hand, catalytic and adsorption properties of open Ln^{III}-ion sites formed on cyano-bridged heterometallic coordination polymers are tunable by combining metal ions by the electronic interaction through CN^- ligands, as discussed in the previous reports using the coordination polymers as heterogeneous hydrolytic catalysts.[38-39] The correlation between catalytic activity and adsorbed species on the surfaces of the catalysts is scrutinized by ex-situ IR measurements after the catalytic reactions.

MATERIALS AND METHODS

Materials. All chemicals were used as delivered. Aqueous solutions were prepared with ultrapure water provided by a Barnstead Smart2Pure water purification system (Thermo Scientific, US), where the electronic conductance was 18.2 $M\Omega$ cm throughout the experiments. Potassium hexacyanocobaltate(III), potassium hexacyanoruthenate(II) hydrate, iron(III) nitrate nonahydrate, terbium(III) nitrate hexahydrate, europium(III) nitrate hexahydrate, cobalt(II) nitrate hexahydrate, terbium(III) oxide ($Tb^{III}_2O_3$), europium(III) oxide ($Eu^{III}_2O_3$), disodium *p*-nitrophenyl phosphate hexahydrate, *p*-nitrophenol, and sodium hydroxide were purchased from FUJIFILM-Wako Pure Chemical Industries Corporation. Silica-alumina (grade 135) and 2-[4-(2-hydroxyethyl)-1-piperazinyl]ethanesulfonic acid (HEPES) were obtained from Sigma-Aldrich Co. LLC. (US). $Tb^{III}_2O_3$ and $Eu^{III}_2O_3$ were treated at 100 °C for 2 h *in vacuo* to remove physiosorbed water. $Fe^{III}[Co^{III}(CN)_6]$ (**FeCo**) and $[Fe^{III}(H_2O)_{3/2}]_{4/3}[Ru^{II}(CN)_6]$ (**FeRu**) were synthesized according to literature procedures.[38, 40]

Immobilization of Lanthanoid Ions on Silica-alumina (Tb^{III}/Al-SiO$_2$ and Eu^{III}/Al-SiO$_2$). Silica-alumina (grade 135, 0.1 g) immersed in an aqueous solution of Ln^{III}(NO$_3$)$_3$ (Ln = Tb or Eu, 0.01 M, 5 mL) was magnetically stirred for 24 h at room temperature. The silica-alumina was collected by centrifugation and washed with water (10 mL) at least three times followed by drying *in vacuo* at room temperature to obtain Tb^{III}/Al-SiO$_2$ and Eu^{III}/Al-SiO$_2$. Molar ratios determined by X-ray fluorescence: Tb/Si = 0.024 for Tb^{III}/Al-SiO$_2$; Eu/Si = 0.026 for Eu^{III}/Al-SiO$_2$.

Synthesis of Lanthanoid Hexacyanocobaltate. An aqueous solution of potassium hexacyanometallate (III) (K$_3$[Co^{III}(CN)$_6$], 0.10 M, 3.0 mL) was slowly added to an aqueous solution of Ln^{III}(NO$_3$)$_3$ (0.13 M, 3.0 mL) with vigorous stirring for 18 h. The formed precipitates were collected by centrifugation and washed with distilled water a few times. The precipitates were dried *in vacuo* for 12 h. Molar ratios determined by X-ray fluorescence: Tb/Co = 1:1 for terbium hexacyanocobaltate (**TbCo**); Eu/Co = 1.0 for euporium hexacyanocobaltate (**EuCo**).

Synthesis of Lanthanoid Hexacyanoruthenate. An aqueous solution of potassium hexacyanoruthenate (II) (K$_4$[Ru^{II}(CN)$_6$], 0.10 M, 3.0 mL) was slowly added to an aqueous solution of Ln^{III}(NO$_3$)$_3$ (0.10 M, 3.0 mL) with vigorous stirring for 18 h. The formed precipitates were collected by centrifugation and washed with distilled water a couple of times. The precipitates were dried *in vacuo* for 12 h. Molar ratios determined by X-ray fluorescence: Tb/Ru = 1.5 for terbium hexacyanoruthenate (**TbRu**); Eu/Ru = 1.4 for europium hexacyanoruthenate (**EuRu**).

Physical Measurements. Ultraviolet−visible (UV−vis) absorption spectra were recorded on a spectrometer, JASCO V−770 (JASCO, Japan). Infrared (IR) spectra were obtained on a spectrometer, FT/IR−6200 (JASCO, Japan) with an attenuated total reflectance unit using a diamond window. Powder X-ray diffraction patterns were recorded on a diffractometer, MiniFlex 600 (Rigaku, Japan). Incident X-ray radiation was produced by a Cu X-ray tube operating at 40

kV and 15 mA with Cu Kα radiation (λ = 1.54 Å). The scan rate was 5° min^{-1} from 2θ = 15−55°. The atomic ratio of heterometallic coordination polymers was determined using an X-ray fluorescence spectrometer, Epsilon 1 (Malvern PANalytical, Netherlands). Dynamic light scattering (DLS) experiments were conducted at room temperature using a Zetasizer Nano S90 (Malvern PANalytical, Netherlands).

Nitrogen (N$_2$) adsorption-desorption isotherms at −196 °C were obtained with a Belsorp-mini II (MicrotracBEL, Japan). Weighed samples (~100 mg) were used for adsorption analysis after pretreatment at 200 °C for 2 h *in vacuo*. The samples were exposed to N$_2$ within a relative pressure range from 0.01 to 101.3 kPa. The adsorbed amount of N$_2$ was calculated from the pressure change in a cell after reaching equilibrium at −196 °C. The total and external surfaces areas were calculated from the Brunauer–Emmett–Teller (BET) plot and *t*-plot, respectively.

Catalysis Evaluation for the Hydrolysis of *p*-Nitrophenyl Phosphate. A typical procedure for catalysis measurements is as follows: a mixed solution of HEPES/NaOH buffer solution (0.1 M, pH 7.0) and ethanol (3:7 v/v, 0.75 mL) containing disodium *p*-nitrophenyl phosphate (*p*-NPP, 25 mM) and a catalyst in a sealed microtube was magnetically stirred at 900 rpm at 60 °C. The concentration of Ln^{III} on the catalyst surfaces was fixed at 0.25 mM to compare the net activities of Ln^{III} for each reaction. An aliquot (10 μL) sampled periodically from the reaction mixture was diluted with a HEPES/NaOH buffer solution (2,490 μL, 0.1 M, pH 8.3) and analyzed by a UV−vis spectrophotometer. The conversion of *p*-NPP at a certain reaction time was determined by the absorbance change at 400 nm ascribed to *p*-nitrophenolate ion (*p*-NP, ε = 1.57 × 10^4 M^{-1} cm).

RESULTS AND DISCUSSION

Homogeneous Catalysis of Trivalent Lanthanoid Ions (Ln[III], Ln = Tb or Eu) for the Hydrolysis of *p*-Nitrophenyl Phosphate. Homogeneous catalysis of trivalent terbium ion (Tb[III]) and europium ion (Eu[III]) for hydrolysis of *p*-nitrophenyl phosphate (*p*-NPP) was examined at 60 °C in a mixed solution of 2-[4-(2-hydroxyethyl)piperazin-1-yl]ethanesulfonate (HEPES/NaOH) buffer solution (0.1 M, pH 7.0) and ethanol (3:7 (v/v), 0.75 mL) containing lanthanoid nitrate (Ln[III](NO$_3$)$_3$, 0.25 mM) and *p*-NPP (25 mM). The yield of the hydrolysis product, *p*-nitrophenolate ion (*p*-NP), was determined by the absorbance change at 400 nm (Figure 2a). Tb[III] and Eu[III]
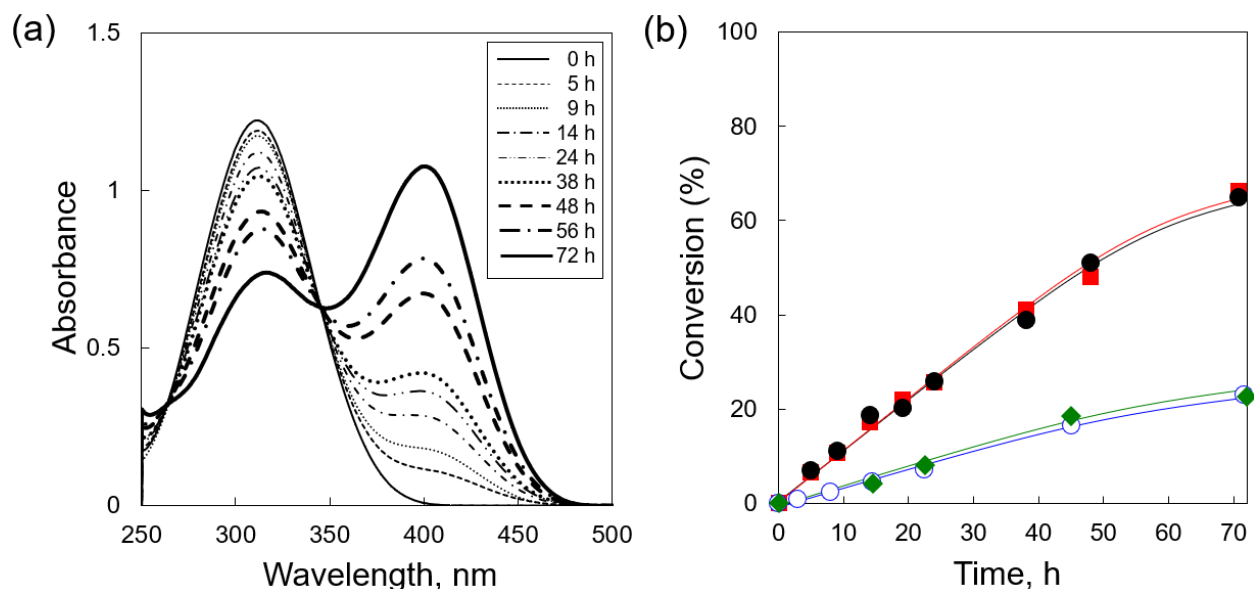
Figure 2. (a) Change of UV-visible spectra of a mixed solution of HEPES/NaOH buffer solution (0.1 M, pH 7.0) and ethanol (3:7 v/v, 0.75 mL) containing disodium *p*-nitrophenyl phosphate (*p*-NPP, 25 mM) at 60 °C in the presence of terbium nitrate (Tb[III](NO$_3$)$_3$, 0.25 mM). (b) Time profiles of *p*-NPP conversion to *p*-nitrophenolate ion (*p*-NP) in the absence (○) or presence of trivalent terbium (Tb[III]) ion (●), europium (Eu[III]) ion (■) or iron (Fe[III]) ion (◆).

ions exhibited comparable activity for the hydrolysis of p-NPP with the conversions of 65% and 64% for 72 h, respectively, which were 2.5 times higher than those with trivalent 3d-metal ions such as Fe^{III} ions and without catalysts (25% and 24% for 72 h, respectively, Figure 2b). The initial (<1 h) reaction rates (v_0) for the reaction systems containing Tb^{III} and Eu^{III} ions were 3.0×10^{-4} mol L^{-1} h^{-1} and 3.1×10^{-4} mol L^{-1} h^{-1}, which were three times faster than those with Fe^{III} ions and without catalysts (7.6×10^{-5} mol L^{-1} h^{-1} and 9.1×10^{-5} mol L^{-1} h^{-1}, respectively).

Heterogeneous Catalysis of Lanthanoid(III) Oxides and Silica-Alumina Containing Ln^{III} Ions for the Hydrolysis of p-Nitrophenyl Phosphate. Heterogenization of the Ln^{III}-ion catalysts (Ln = Tb or Eu) was carried out by preparation of lanthanoid oxides ($Ln^{III}_2O_3$) and immobilization of Ln^{III} ions on silica-alumina by cation exchange method (Ln^{III}/Al-SiO$_2$, Ln = Tb or Eu). The amounts of Tb and Eu atoms immobilized on Tb^{III}/Al-SiO$_2$ and Eu^{III}/Al-SiO$_2$ were 0.033 mol g^{-1} and 0.036 mol g^{-1}, respectively, as determined by the X-ray fluorescence analyses.

Nitrogen (N_2) adsorption-desorption measurements were performed to determine the specific surface areas of the obtained catalysts. The type III isotherms were observed for $Tb^{III}_2O_3$ and $Eu^{III}_2O_3$, indicating the absence of interior micropores and mesopores (Figure S1a, b). The total surface areas calculated from the Brunauer–Emmett–Teller (BET) method were 5 and 9 m^2 g^{-1} for $Tb^{III}_2O_3$ and $Eu^{III}_2O_3$, respectively (Table 1). The type IV isotherm observed for Al-SiO$_2$ indicated the presence of interior mesopores (Figure S1c). The total surface areas calculated from the BET method and the external surface area calculated from t-plot were 361 and 8 m^2 g^{-1}, respectively. The size of p-NPP (ca. 10 Å) is smaller than the mesopores of Al-SiO$_2$, indicating that the Ln^{III} ions distributed on the interior surface work as active sites as well as those on the external surface.

Table 1. Molar ratios of metal ions determined by X-ray fluorescence measurements, and total, microporous and external surface areas calculated from nitrogen (N_2) adsorption-desorption isotherms of lanthanum oxides, silica-alumina, and cyano-bridged heterometallic coordination polymers[a]

	Total surface area[b], $m^2\ g^{-1}$	Microporous surface area[c], $m^2\ g^{-1}$	External surface area[c], $m^2\ g^{-1}$
Terbium oxide ($Tb^{III}_2O_3$)	5	–	5
Europium oxide ($Eu^{III}_2O_3$)	9	–	9
Silica-alumina (Al-SiO_2)	361	353	8
TbCo	4	–	4
TbRu	5	–	5
EuCo	4	–	4
EuRu	6	–	6
FeCo	135	112	23
FeRu	213	195	18

a. N_2 adsorption-desorption isotherms are shown in Figure S1.
b. Total surface areas were obtained by the Brunauer−Emmett−Teller (BET) method.
c. Microporous and external surface areas were calculated by *t*-plot.

Catalytic activity of the heterogeneous catalysts was examined for the hydrolysis of *p*-NPP at 60 °C in a mixed solution of HEPES/NaOH buffer solution (0.1 M, pH 7.0) and ethanol (3:7 v/v, 0.75 mL) containing the heterogeneous catalysts ([Ln^{III}] = 0.25 mM) and *p*-NPP (25 mM). The conversions for 72 h for the reaction systems containing $Tb^{III}_2O_3$ (57%), $Eu^{III}_2O_3$ (52%), Tb^{III}/Al-SiO_2 (50%) and Eu^{III}/Al-SiO_2 (51%) were all lower than those of corresponding Ln^{III} ions acting as homogeneous catalysts in the reaction solutions (65% and 64% for Tb^{III} and Eu^{III} ions, respectively; Figure 3a and b). On the other hand, the v_0s for the reaction systems containing $Tb^{III}_2O_3$ (2.8×10^{-4} mol L^{-1} h^{-1}), $Eu^{III}_2O_3$ (3.3×10^{-4} mol L^{-1} h^{-1}), Tb^{III}/Al-SiO_2 (3.0×10^{-4} mol L^{-1} h^{-1}) and Eu^{III}/Al-SiO_2 (3.0×10^{-4} mol L^{-1} h^{-1}) were comparable to those of corresponding Ln^{III} ions (3.0×10^{-4} mol L^{-1} h^{-1} and 3.1×10^{-4} mol L^{-1} h^{-1} for Tb^{III} and Eu^{III} ions, respectively).
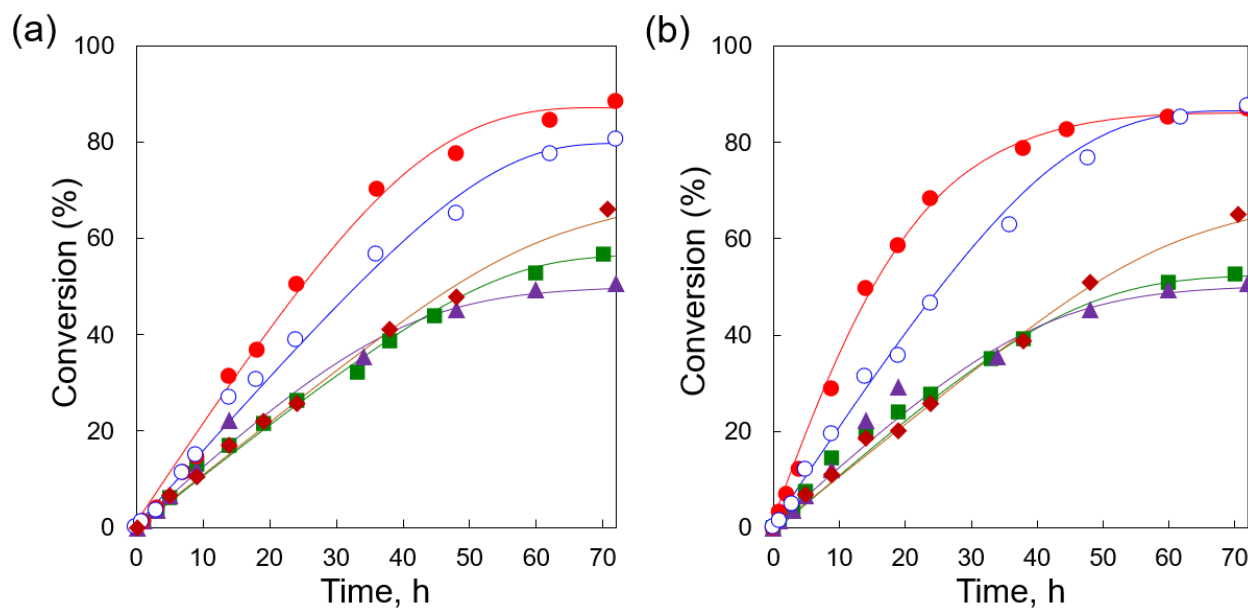
Figure 3. (a) Time profiles of the *p*-nitrophenyl phosphate (*p*-NPP) conversion to *p*-nitrophenolate ion (*p*-NP) in a mixed solution of HEPES/NaOH buffer solution (0.1 M, pH 7.0) and ethanol (3:7 v/v, 0.75 mL) containing disodium *p*-nitrophenyl phosphate (*p*-NPP, 25 mM) at 60 °C in the presence of terbium oxide (Tb$^{III}_2$O$_3$, ■), terbium ion immobilized on silica-alumina (Tb^{III}/Al-SiO$_2$, ▲), terbium hexacyanocobaltate (**TbCo**, ●), terbium hexacyanoruthenate (**TbRu**, ○), and terbium nitrate (◆). (b) Time profiles of the *p*-NPP conversion to *p*-NP in a mixed solution of HEPES/NaOH buffer solution (0.1 M, pH 7.0) and ethanol (3:7 v/v, 0.75 mL) containing *p*-NPP (25 mM) at 60 °C in the presence of europium oxide (Eu$^{III}_2$O$_3$,■), europium ion immobilized on silica-alumina (Eu^{III}/Al-SiO$_2$, ▲), europium hexacyanocobaltate (**EuCo**, ●), europium hexacyanoruthenate (**EuRu**, ○) and europium nitrate (◆).

The reasons for the low catalytic activity of Ln$^{III}_2$O$_3$ and Ln^{III}/Al-SiO$_2$ (Ln = Tb or Eu) were confirmed by ex-situ infrared (IR) spectroscopy. Ln$^{III}_2$O$_3$ and Ln^{III}/Al-SiO$_2$ after the catalytic reactions exhibited peaks assignable to PO stretching (ν_{PO}) bands (1020-1063 cm^{-1}) of dihydrogen phosphate (H$_2$PO$_4^-$) appeared after the catalytic reactions, although the peaks for Ln^{III}/Al-SiO$_2$

after the catalytic reactions were not obvious due to the overlapping with SiO stretching (ν_{SiO}) bands (ca. 1030 cm^{-1}) of Al-SiO$_2$ (Figure 4a-d). The results indicate that the low catalytic activity
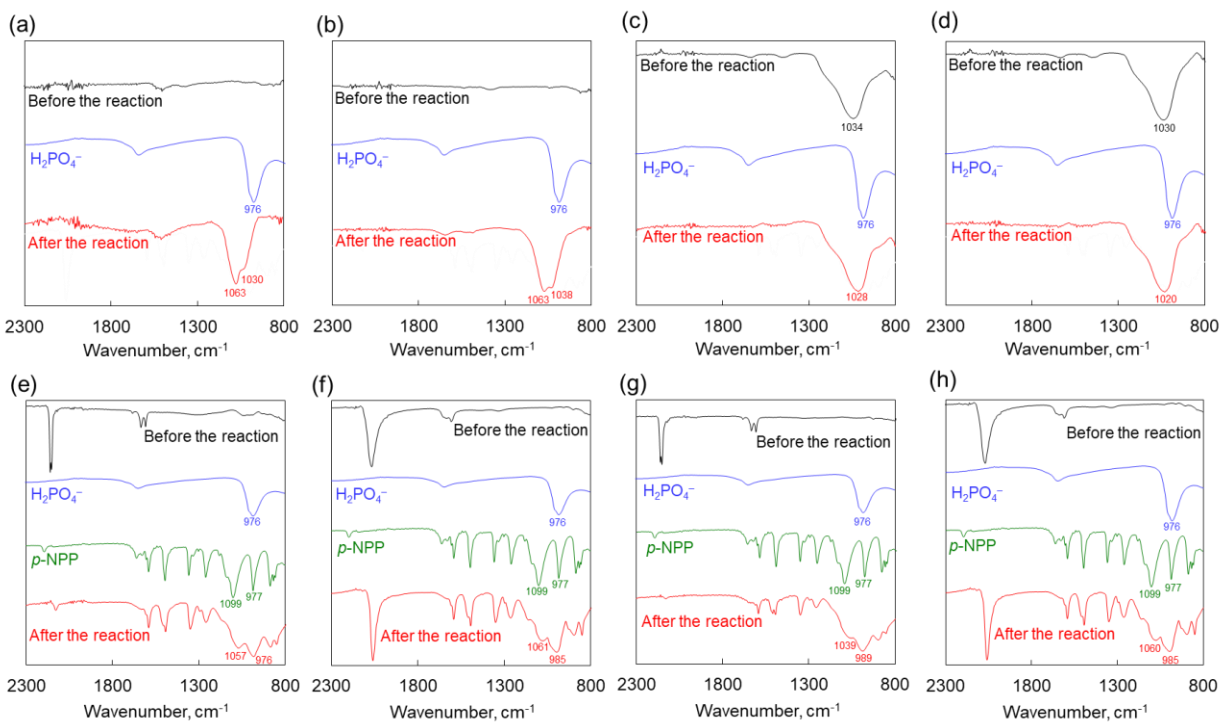
Figure 4. Infrared (IR) spectra of (a) terbium oxide (Tb$^{III}_2$O$_3$), (b) europium oxide (Eu$^{III}_2$O$_3$), (c) Tb^{III}/Al-SiO$_2$, (d) Eu^{III}/Al-SiO$_2$, (e) terbium hexacyanocobaltate (**TbCo**), (f) terbium hexacyanoruthenate (**TbRu**), (g) europium hexacyanocobaltate (**EuCo**), and (h) europium hexacyanoruthenate (**EuRu**) after the catalytic hydrolysis of *p*-nitrophenyl phosphate (*p*-NPP, 25 mM) in a mixed solution of HEPES/NaOH buffer solution (0.1 M, pH 7.0) and ethanol (3:7 v/v, 0.75 mL) at 60 °C.

resulted from the product inhibition by the specific adsorption of H$_2$PO$_4{}^-$.

Heterogeneous Catalysis of Cyano-bridged Heterometallic Coordination Polymers Containing N-bound Ln^{III} Ions for the Hydrolysis of *p*-Nitrophenyl Phosphate. Not only

simple heterogenization but also tuning of interaction between Ln^{III} ions and *p*-NPP is essential for the enhancement of heterogeneous catalysis for the hydrolysis of *p*-NPP. In this context, cyano-bridged heterometallic coordination polymers are strong candidates for the heterogenization of Ln^{III}-ion catalysts. The formula of cyano-bridged heterometallic coordination polymers can be described as $[Ln^{III}(H_2O)_x]_y[M^C(CN)_6]$, where M^C represents the C-bound metal ions.[41–45] Open sites are formed on Ln^{III} ions after the liberation of aqua ligands. The catalytic and adsorption properties of open Ln^{III} ion are manipulated by the coupled M^C ions through conjugated CN^- ligands.[38-39] Herein, trivalent Co^{III} and divalent Ru^{II} ions are chosen as the M^C ions to examine the effect of oxidation states of M^C ions on the catalytic and adsorption properties.

A series of cyano-bridged heterometallic coordination polymers, terbium hexacyanocobaltate (**TbCo**), terbium hexacyanoruthenate (**TbRu**), europium hexacyanocobaltate (**EuCo**), and europium hexacyanoruthenate (**EuRu**), were synthesized by mixing an aqueous solution containing $Ln^{III}(NO_3)_3$ and an aqueous solution of potassium hexacyanometallate ($K_3[Co^{III}(CN)_6]$ or $K_4[Ru^{II}(CN)_6]$) to yield precipitates. The molar ratio of M^N/M^C of each **LnM^C** (Ln = Tb or Eu; M^C = Co or Ru) determined by X-ray fluorescence spectroscopy was virtually the same as the theoretical formulae of the coordination polymers under consideration of the charge compensation. The scanning electron microscope (SEM) images showed that the particles size of each coordination polymer was less than 20 μm (Figure S2). No shape-controlled particles were obtained for **TbRu** and **EuRu**. On the other hand, the particles of **TbCo** and **EuCo** were grown to a rod-like shape.[46] However, the morphology of the heterometallic coordination polymers insignificantly affected the crystal structure and heterogeneous catalysis, as described below.

LnCos (Ln = Tb or Eu) provided powder X-ray diffraction (PXRD) patterns comparable to the simulated pattern of $[Eu^{III}(H_2O)_2][Fe^{III}(CN)_6]\cdot2H_2O$ in the space group *Cmcm* calculated from the

crystal structure, indicating that the formulae of **LnCo**s can be described as [$Ln^{III}(H_2O)_2$][$Co^{III}(CN)_6$]·$2H_2O$ (Figure 5a).[47] The Ln^{III} ions in **LnCo**s in a square antiprismatic geometry is coordinated by six N atoms of the CN^- ligands and two O atoms of the aqua ligands. On the other hand, **LnRu**s (Ln = Tb or Eu) provided the PXRD patterns comparable to the simulated pattern of [$La^{III}(H_2O)_3$][$Fe^{III}(CN)_6$]·$2H_2O$ in the space group $P6_3/m$, where the Ln^{III} ions are in a tricapped trigonal prism geometry (Figure 5b).[48] The chemical formulae of **LnRu**s can be estimated as [$Ln^{III}(H_2O)_{9/2}$]$_{4/3}$[$Ru^{II}(CN)_6$]·$2H_2O$ under consideration of the charge compensation. Open Ln^{III} ion sites available as catalytic active sites can be formed in both **LnCo**s and **LnRu**s by liberation of the aqua ligands. On the other hand, the C-bound Co^{III} and Ru^{II} ions hardly act as active sites due to their coordinative saturation.

The bridging structures of M^C–CN–M^N in the coordination polymers were confirmed by infrared (IR) spectroscopy. CN-stretching (ν_{CN}) bands of **LnM^C**s shifted from those of K_3[$Co^{III}(CN)_6$] (2125 cm^{-1}) and K_4[$Ru^{II}(CN)_6$] (2054 cm^{-1}) in the higher wavenumber region (Figure S3). Such higher wavenumber shift evidenced the formation of M^C–CN–M^N bridging structures because the electron density of an antibonding sigma (σ*) orbital of CN ligand was reduced by the coordination to Ln^{III} ions.[49] Two ν_{CN}s of **TbCo** (2154 and 2162 cm^{-1}) resulted from the involvement of two crystallographically-independent CN^- moieties as observed in the crystal structure of [$Eu^{III}(H_2O)_2$][$Fe^{III}(CN)_6$]·$2H_2O$.[47] ν_{CN}s of **EuCo** (2150 and 2158 cm^{-1}) slightly shifted from those of **TbCo** in the lower-wavenumber region because the electron density of an σ* orbital was reduced by Tb^{III} ions with smaller ionic radii compared with Eu^{III} ions by the lanthanoid contraction.[50-51] Single ν_{CN} peaks observed for **TbRu** and **EuRu** (2065 and 2069 cm^{-1}, respectively) because all CN^- moieties are crystallographically equivalent as evidenced by the crystal structure of [$La^{III}(H_2O)_3$][$Fe^{III}(CN)_6$]·$2H_2O$.[48] ν_{CN}s of **TbRu** and **EuRu** shifted from those
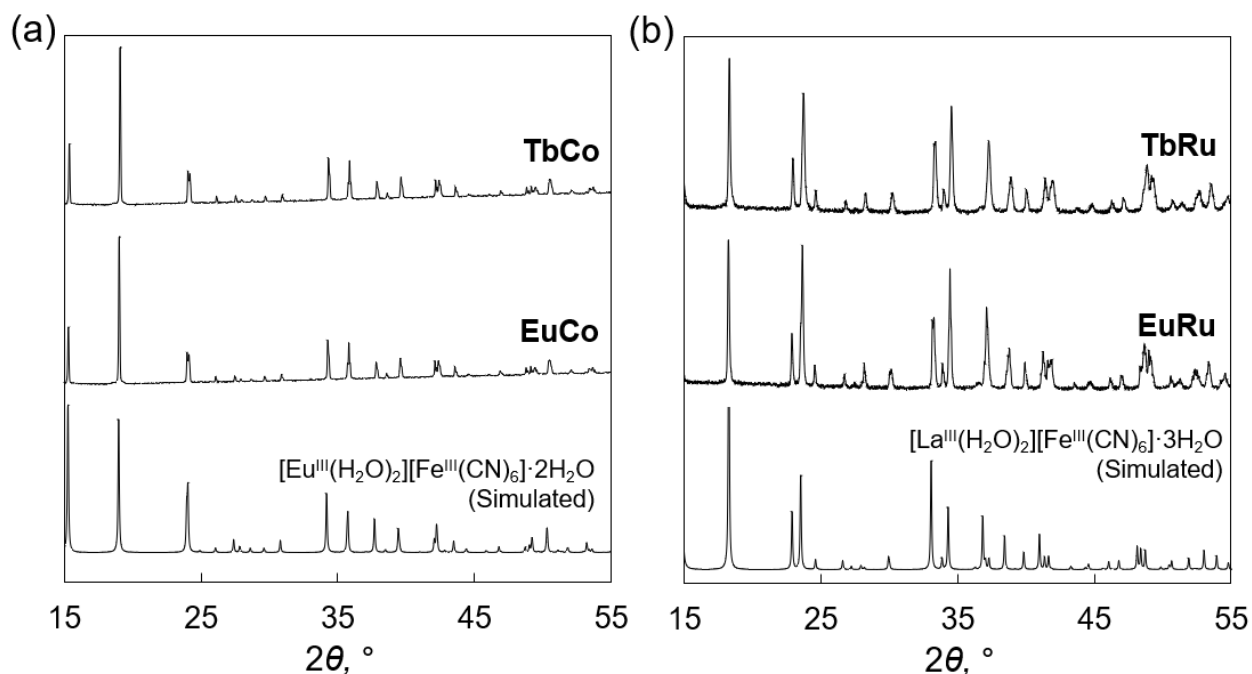
Figure 5. (a) Observed powder X-ray diffraction (PXRD) patterns ($2\theta = 15-55°$) of terbium hexacyanocobaltate (**TbCo**), europium hexacyanocobaltate (**EuCo**), and simulated PXRD pattern of europium hexacyanoferrate tetrahydrate ($[Eu^{III}(H_2O)_2][Fe^{III}(CN)_6]\cdot2H_2O$) calculated from the deposited crystal structure (CCDC deposition No. 992673). (b) Observed PXRD patterns of terbium hexacyanoruthenate (**TbRu**), europium hexacyanoruthenate (**EuRu**), and simulated PXRD pattern of lanthanum hexacyanoferrate pentahydrate ($[La^{III}(H_2O)_3][Fe^{III}(CN)_6]\cdot2H_2O$) calculated from the deposited crystal structure (CCDC deposition No. 1592456).

of **TbCo** and **EuCo** (≥2150 cm^{-1}) in the lower-wavenumber region because the electron density of an σ* orbital was reduced by the coordination to trivalent Co^{III} ions compared with divalent Ru^{II} ions.[52]

Nitrogen (N$_2$) adsorption-desorption measurements were performed to investigate the surface areas of **LnM^C**s (Ln = Tb or Ru; M^C = Fe or Ru) (Figure S1d–g). The type III isotherms observed

for **LnM^C**s indicated the absence of interior micropores and mesopores. The total surface areas for

LnM^{C}s calculated from the Brunauer–Emmett–Teller (BET) method were 4, 5, 4, and 6 m^2 g^{-1} for

TbCo, **TbRu**, **EuCo**, and **EuRu**, respectively (Table 1). Micropores of **LnM^C**s (< 4 Å) estimated

from the crystal structures hardly allow penetration of N$_2$ molecules, resulting in a low amount of

N$_2$ adsorption.[47-48] The size of *p*-nitrophenyl phosphate (*p*-NPP, ca. 10 Å) is larger than the

micropores of **LnM^C**s, indicating that the Ln^{III} ions available as active sites are distributed on the

external surfaces of **LnM^C**s particles.

The catalytic activity of **LnM^C**s ([Ln^{III}] = 0.25 mM) was examined for the hydrolysis of *p*-NPP

(25 mM). The conversions for the reactions in the presence of **TbCo**, **TbRu**, **EuCo**, and **EuRu**

(88%, 80%, 88%, and 88% for 72 h, respectively) were all higher than those of Ln^{III}$_2$O$_3$ (~55%),

Ln^{III}/Al-SiO$_2$ (~50%), and Ln^{III}(NO$_3$)$_3$ (~65%) (Figure 3a and b). **TbCo** and **EuCo** exhibited

higher v_0s (3.4 × 10^{-4} mol L^{-1} h^{-1}and 8.7 × 10^{-4} mol L^{-1} h^{-1}, respectively) compared with the

corresponding **LnRu**s (3.0 × 10^{-4} mol L^{-1} h^{-1} and 4.0 × 10^{-4} mol L^{-1} h^{-1} for **TbRu** and **EuRu**,

respectively), because of the enhanced surface acidity of the coordination polymers by trivalent

Co^{III} ions compared with divalent Ru^{II} ions.[38]

Reasons for high conversions of **LnM^C**s were confirmed by ex-situ IR spectroscopy. IR

measurements of **LnM^C**s clarified that the broad v_{PO} peaks assignable to H$_2$PO$_4$$^-$ and sharp v_{PO}

peaks assignable to *p*-NPP appeared after the catalytic reaction (Figure 4e−h). Non-selective

adsorption of H$_2$PO$_4$$^-$ indicates that the product inhibition hardly occurred for **LnM^C**s during the

hydrolysis of *p*-NPP. The properties of the open Ln^{III}-ion sites are affected by the electronic

interactions between the C-bound metal ions, resulting in enhancement of the adsorption ability of

Ln^{III} ions for *p*-NPP. Such electronic interactions that enhance *p*-NPP adsorption cannot be

expected for Ln^{III}$_2$O$_3$ and Ln^{III}/Al-SiO$_2$. The v_{PO} peaks at 1099 and 977 cm^{-1} for *p*-NPP dissolved

in the reaction solution are assignable to asymmetric and symmetric v_{PO}, respectively (Figure 4e−h, green lines).[53,54] The asymmetric and symmetric v_{PO} peaks observed for **LnM^C**s after the reactions slightly shifted to lower and higher wavenumber sides, respectively, from those of *p*-NPP in the solution (1057 and 976 cm^{-1} for **TbCo**, 1061 and 985 cm^{-1} for **TbRu**, 1039 and 989 cm^{-1} for **EuCo**, and 1060 and 985 cm^{-1} for **EuRu**), although symmetric v_{PO} peaks were not obvious due to the overlap with the broad v_{PO} peaks of $H_2PO_4^-$. The shifts resulted from the significant distortions of PO bonds by forming coordination bonds with metal ions and hydrogen bonds with water coordinating to the metal ion, as evidenced by the spectroscopic studies on organophosphate adsorption on goethite and uranium(IV) hydroxide.[55,56] The estimated formulae of **LnM^C**s are $[Ln^{III}(H_2O)_3][Co^{III}(CN)_6]$ or $[Ln^{III}(H_2O)_{9/2}]_{4/3}[Ru^{II}(CN)_6]$, indicating that open sites (≥3) are formed on each Ln^{III} ion available as adsorption sites of *p*-NPP and water. The strong interaction between adsorbed *p*-NPP and water on a Ln^{III} ion resulted in acceleration of the hydrolysis of *p*-NPP on the surface of **LnM^C**s.

Catalysis Comparison of Cyano-bridged Heterometallic Coordination Polymers Composed of Ln^{III} Ions with Other Catalysts. The high activity of **LnM^C**s was manifested by the catalysis comparison with cyano-bridged heterometallic coordination polymers containing 3d-metal ions as N-bound metal ions. Iron(III) ion was chosen as the M^N ion because of its high activity among 3d-metal ions, as reported previously.[38] Iron(III) hexacyanocobaltate (**FeCo**) and iron(III) hexacyanoruthenate (**FeRu**) were synthesized according to the reported procedures.[38, 40] The total surface areas for **FeCo** and **FeRu** calculated from the BET method based on their N_2 adsorption-desorption isotherms were 135 and 213 m^2 g^{-1}, respectively (Table 1 and Figure S2h–i). The external surface areas for **FeCo** and **FeRu** calculated from the *t*-plot method were 23 and 18 m^2 g^{-1}, respectively.

The activity of **FeRu** ($[Fe^{III}]$ = 0.25 mM) as a heterogeneous catalyst was examined for the hydrolysis of *p*-NPP (25 mM). The conversion for 72 h and v_0 of **FeRu** (36% and 1.6×10^{-4} mol L^{-1} h^{-1}, respectively) were lower than those of **LnM^C**s owing to the stronger Lewis acidity of Ln^{III} ions than Fe^{III} ions (Figure 6). The activity of **FeCo** ($[Fe^{III}]$ = 0.25 mM) as a heterogeneous catalyst was also examined in the same reaction conditions; however, the formation of *p*-NP was observed even after removing **FeCo** from the reaction solution (Figure S4). Several cyano-bridged coordination polymers having a colloidal nature act as homogeneous catalysts.[57−60] IR spectrum of the supernatant indicates that colloidal **FeCo** particles were dispersed in the supernatant without decomposition to $[Co^{III}(CN)_6]^{3-}$ ions (Figure S5). The size of colloidal **FeCo** particles in the supernatant was estimated to be several tens nm by the dynamic light scattering (DLS) measurement (Figure S6a), which was much smaller than **FeCo** particles removed from the reaction solution (>400 nm, Figure S6b). Thus, the colloidal **FeCo** particles formed during the reaction worked as a catalyst for the hydrolysis of *p*-NPP. These results indicate that the incorporation of Ln^{III} ions contributes to the enhancement of the heterogeneous catalytic activity as well as durability of cyano-bridged heterometallic coordination polymers compared with the incorporation of Fe^{III} ions.

Catalytic performance of reported catalysts containing Ln ions was summarized in Table S1 in terms of conversions, half-life times ($t_{1/2}$s) of organophosphates, and turn-over frequencies (TOFs) for the hydrolysis of various organophosphates, although the organophosphates examined in the previous studies have slightly different reactivity from *p*-NPP. The values shown in Table S1 were obtained at the optimum pH and temperature of each catalyst. The TOFs were calculated using the initial (≤1 h) reaction rate (v_0) and the concentration of Ln ions in each reaction system to compare
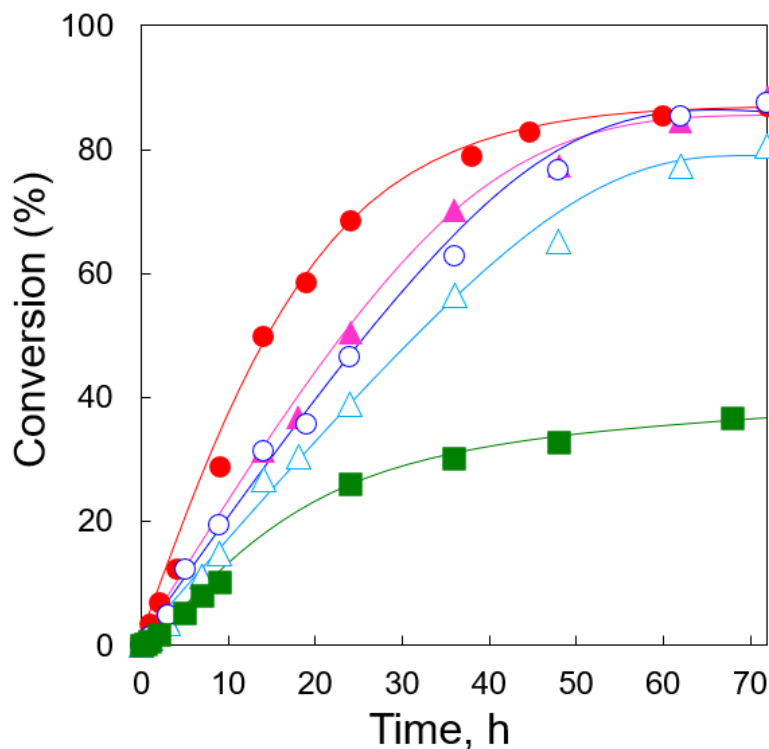
Figure 6. Time profiles of the *p*-nitrophenyl phosphate (*p*-NPP) conversion to *p*-nitrophenolate ion (*p*-NP) in a mixed solution of HEPES/NaOH buffer solution (0.1 M, pH 7.0) and ethanol (3:7 v/v, 0.75 mL) containing disodium *p*-nitrophenyl phosphate (*p*-NPP, 25 mM) at 60 °C in the presence of terbium hexacyanocobaltate (**TbCo**, ▲), terbium hexacyanoruthenate (**TbRu**, △), europium hexacyanocobaltate (**EuCo**, ●), europium hexacyanoruthenate (**EuRu**, ○), or iron hexacyanoruthenate (**FeRu**, ■).

the net activities of Ln ions. $t_{1/2}$s in the reaction systems containing **LnM^{C}s** (≤24 h, [Ln]/[substrate] = 1%, entry 10–13) were much shorter than those containing the reported coordination polymer catalysts for the hydrolysis of bis(*p*-nitrophenyl)phosphate (≥3.4 days) even in the presence of the high concentration of Ln ions ([Ln]/[substrate] ≥10%, entry 1-4).[61–63] TOFs of the reaction systems containing $Ln^{III}_{0.33}[Ln^{III}_4(OH)_4(OAc)_3(H_2O)_7][Rh_4Zn_4O(L\text{-cysteine})_{12}]$ were ~0.23 for the

18

hydrolysis of p-NPP ([Ln]/[p-NPP] = 22%, entry 5), which was lower than those of **EuCo** (3.3 h^{-1}, entry 11).[64] An exceptional example is Ce$^{IV}_6$O$_4$(OH)$_4$(1,4-benzenedicarboxylate)$_6$ ([Ce^{IV}]/[dimethyl p-nitrophenyl phosphate] = 36%) with the conversion of 88% for 1 h, $t_{1/2}$ of 8 min, and TOFs of 2.4 h^{-1}, which are benchmark values in the hydrolysis of organophosphates by Ln catalysts (entry 6).[36] However, such a high activity is observed only in highly basic conditions with high catalyst concentrations. **EuCo** exhibited the comparable TOF with Ce$^{IV}_6$O$_4$(OH)$_4$(1,4-benzenedicarboxylate)$_6$ at neutral pH (3.3 h^{-1}, entry 11) with low catalyst concentration as 1%, manifesting that choice of coordination polymers would enable to remove organophosphates at various pH conditions.

The high activity of **LnM^{C}s** for the hydrolysis of p-NPP was evidenced by the comparison to catalysts other than coordination polymers in the reaction systems with [Ln]/[p-NPP] ratio of 1%. The conversion of p-NPP and TOF in the reaction system containing **EuCo** (88% for 3 days and 3.3 h^{-1}, respectively, entry 11) were much higher than those containing Eu^{III}(cryptate[2.2.1])Cl$_3$ (4% for 3.8 days and 0.075 h^{-1}, entry 7), [Gd^{III}(OAc)$_3$(H$_2$O)$_2$]$_2$ (2% for 2 h and 1.0 h^{-1}, entry 8) and La^{III} ions immobilized on hectorite (20% for 8.7 days, 0.17 h^{-1}, entry 9).[65–67] Ex-situ IR and mass spectroscopic analyses indicated that the low activity resulted from strong adsorption of (di)hydrogen phosphate as well as Ln$^{III}_2$O$_3$ and Ln^{III}/Al-SiO$_2$ in our study.

CONCLUSIONS

Heterogenization of trivalent lanthanoid-ion (Ln^{III}, Ln = Tb or Eu) catalysts was investigated to enhance the catalytic activity for the hydrolysis of p-nitrophenyl phosphate (p-NPP). The heterogenization was carried out by the preparation of lanthanoid oxides (Ln$^{III}_2$O$_3$), the immobilization of the Ln^{III} ions on silica-alumina, and the synthesis of cyano-bridged heterometallic coordination polymers containing Ln^{III} ions as the N-bound metal ions

([Ln^{III}(H$_2$O)$_x$]$_y$[M^C(CN)$_6$], Ln = Tb or Eu; M^C = Fe^{III} or Ru^{II}; $x \geq 2$). The higher initial reaction rates (v_0) and conversions of p-NPP were observed in the reactions using **LnM^C**s as heterogeneous catalysts compared with those using Ln^{III}$_2$O$_3$ and silica-alumina immobilizing the Ln^{III} ions. Significantly, **LnCo**s exhibited higher activity than **LnRu**s due to the strong surface Lewis acidity of trivalent C-bound metal ions. The activity of **LnM^C**s was also higher than **FeM^C**s because of the strong Lewis acidity and stability of **LnM^C**s. Ex-situ infrared (IR) spectra of Ln^{III}$_2$O$_3$ and silica-alumina immobilizing Ln^{III} ions were inhibited by the dihydrogen phosphate (H$_2$PO$_4^-$) by the specific adsorption of H$_2$PO$_4^-$. On the other hand, p-NPP preferably interacts with **LnM^C**s because of the change of electronic properties of Ln^{III} ions by the C-bound metal ions through conjugated CN$^-$ ligands. The adsorbed p-NPP on Ln^{III} ions has strong interaction with water coordinating to the Ln^{III} ions, resulting in the acceleration of hydrolysis on the **LnM^C**s surfaces. The basic insight disclosed here is beneficial to develop novel catalysts utilizing Ln^{III} ions in cyano-bridged metal complexes with high activity.

ASSOCIATED CONTENT

Supporting Information

The Supporting Information is available free of charge on the ACS Publications website. Nitrogen (N$_2$) adsorption-desorption isotherms, scanning electron microscope (SEM) images, infrared (IR) spectra, and dynamic light scattering (DLS) data.

Notes

The authors declare no competing financial interest.

The manuscript was written through the contributions of all authors. All authors have given approval to the final version of the manuscript.

ACKNOWLEDGEMENT

REFERENCES

1.   Alozi, M.; Rawas-Qalaji, M., Treating Organophosphates Poisoning: Management Challenges and Potential Solutions. *Crit. Rev. Toxicol.* **2020**, *50*, 764−779.

2.   Parween, T.; Jan, S., *Ecophysiology of Pesticides: Interface between Pesticide Chemistry and Plant Physiology*. 1st Edition ed.; Academic Press: Massachusetts, **2019**.

3.   Worek, F.; Jenner, J.; Thiermann, H., *Chemical Warfare Toxicology: Volume 2: Management of Poisoning,* 1st Edition ed.; Royal Society of Chemistry: UK, **2016**.

4.   Wilkinson, N., *Organophosphorus Pesticides: Structural Characteristics, Mechanisms of Toxicity and Effects of Exposure on Health*. 1st Edition ed.; Nova Science Publishers Inc.: New York, **2016**.

5.   Tang, J.; Ma, X. H.; Yang, J.; Feng, D. D.; Wang, X. Q. Recent Advances in Metal-organic Frameworks for Pesticide Detection and Adsorption. *Dalton Trans.* **2020**, *49*, 14361−14372.

6.   Drout, R. J.; Kato, S.; Chen, H. Y.; Son, F. A.; Otake, K. I.; Islamoglu, T.; Snurr, R. Q.; Farha, O. K. Isothermal Titration Calorimetry to Explore the Parameter Space of Organophosphorus Agrochemical Adsorption in MOFs. *J. Am. Chem. Soc.* **2020**, *142*, 12357−12366.

7.   Zheng, A. X.; Shen, C.; Tang, Q.; Gong, C. B.; Chow, C. F. Catalytic Chemosensing Assay for Selective Detection of Methyl Parathion Organophosphate Pesticide. *Chem. Eur. J.* **2019**, 25, 9643−9649.

8.   Nagpal, M.; Kakkar, R. Use of Metal Oxides for the Adsorptive Removal of Toxic Organic Pollutants. *Sep. Purif. Technol.* **2019**, *211*, 522−539.

9.   Liu, T.; Xu, S. R.; Lu, S. Y.; Qin, P.; Bi, B.; Ding, H. D.; Liu, Y.; Guo, X. C.; Liu, X. H. A Review on Removal of Organophosphorus Pesticides in Constructed Wetland: Performance, Mechanism, and Influencing Factors. *Sci. Total. Environ.* **2019**, *651*, 2247−2268.

10.   Holdren, S.; Tsyshevsky, R.; Fears, K.; Owrutsky, J.; Wu, T.; Wang, X. Z.; Eichhorn, B. W.; Kuklja, M. M.; Zachariah, M. R. Adsorption and Destruction of the G-series Nerve Agent Simulant Dimethyl Methylphosphonate on Zinc Oxide. *ACS Catal.* **2019**, *9*, 902−911.

11.   Zhang, Y.; Yue, Q.; Yu, L.; Yang, X. Y.; Hou, X. F.; Zhao, D. Y.; Cheng, X. W.; Deng, Y. H., Amphiphilic Block Copolymers Directed Interface Coassembly to Construct Multifunctional Microspheres with Magnetic Core and Monolayer Mesoporous Aluminosilicate Shell. *Adv Mater* **2018,** *30*, 1800345.

12.   Wang, W.; Deng, S. B.; Li, D. Y.; Ren, L.; Wang, B.; Huang, J.; Wang, Y. J.; Yu, G., Adsorptive Removal of Organophosphate Flame Retardants from Water by Non-ionic Resins. *Chem. Eng. J.* **2018,** *354*, 105−112.

13. Kim, J.; Li, W.; Philips, B. L.; Grey, C. P., Phosphate Adsorption on the Iron Oxyhydroxides Goethite (alpha-FeOOH), Akaganeite (beta-FeOOH), and Lepidocrocite (gamma-FeOOH): a P-31 NMR Study. *Energ. Environ. Sci.* **2011,** *4*, 4298−4305.

14. Pehkonen, S. O.; Zhang, Q., The degradation of Organophosphorus Pesticides in Natural Waters: A Critical Review. *Crit. Rev. Env. Sci. Technol.* **2002,** *32*, 17−72.

15. Gomes, M. A. G. B.; Fernandes, C.; Gahan, L. R.; Schenk, G.; Horn, A., Recent Advances in Heterogeneous Catalytic Systems Containing Metal Ions for Phosphate Ester Hydrolysis. *Chem. Eur. J.* **2021**, *27*, 877−887.

16. Royuela, S.; Gil-San Millan, R.; Mancheno, M. J.; Ramos, M. M.; Segura, J. L.; Navarro, J. A. R.; Zamora, F. Catalytically Active Imine-based Covalent Organic Frameworks for Detoxification of Nerve Agent Simulants in Aqueous Media. *Materials* **2019**, *12*, 1974−1985.

17. Singh, P.; Borthakur, A.; Mishra, P. K.; Tiwary, D. *Nano-materials as Photocatalysts for Degradation of Environmental Pollutants*. 1st ed.; Elsevier: Netherlands, **2019**.

18. Kumar, S.; Kaushik, G.; Dar, M. A.; Nimesh, S.; Lopez-Chuken, U. J.; Villarreal-Chiu, J. F., Microbial Degradation of Organophosphate Pesticides: A Review. *Pedosphere* **2018,** *28*, 190−208.

19. Raushel, F. M., Catalytic Detoxification. *Nature* **2011,** *469*, 310-311.

20. Parkin, G., Synthetic Analogues Relevant to the Structure and Function of Zinc Enzymes. *Chem. Rev.* **2004,** *104*, 699−767.

21. Weston, J., Mode of Action of Bi- and Trinuclear Zinc Hydrolases and Their Synthetic Analogues. *Chem. Rev.* **2005,** *105*, 2151−2174.

22. Cleland, W. W.; Hengge, A. C., Enzymatic Mechanisms of Phosphate and Sulfate Transfer. *Chem. Rev.* **2006,** *106*, 3252−3278.

23.   Ferri, D.; Barba-Bon, A.; Costero, A. M.; Gaviña, P.; Parraab, M.; Gilab, S., An Au(III)–Amino Alcohol Complex for Degradation of Organophosphorus Pesticides. *RSC Adv.* **2015,** *5*, 106941.

24.   Pehkone, S. O.; Judeh, Z. M., Mechanism of Interactions between Hg(II) and Demeton S: an NMR Study. *Environ. Sci. Technol.* **2005,** *39*, 2586−2591.

25.   Neverov, A. A.; Brown, R. S., Cu(II)-Mediated Decomposition of Phosphorothionate P=S Pesticides. Billion-fold Acceleration of the Methanolysis of Fenitrothion Promoted by a Simple Cu(II)–Ligand System. *Org. Biomol. Chem.* **2004,** *2*, 2245−2248.

26.   Huang, C.; Stone, A. T., Transformation of the Plant Growth Regulator Daminozide (Alar) and Structurally Related Compounds with Cu[II] Ions: Oxidation versus Hydrolysis. *Environ. Sci. Technol.* **2003,** *37*, 1829−1837.

27.   Huang, C.; Stone, A. T., Synergistic Catalysis of Dimetilan Hydrolysis by Metal Ions and Organic Ligands. *Environ. Sci. Technol.* **2000,** *34*, 4117−4122.

28.   Zeinali, M.; Torrents, A., Mercury-Promoted Hydrolysis of Parathion-methyl: Effect of Chloride and Hydrated Species. *Environ. Sci. Technol.* **1998,** *32*, 2238−2342.

29.   Gellman, S. H.; Fetter, R.; Breslow, R., Catalytic Hydrolysis of a Phosphate Triester by Tetracoordinated Zinc Complexes. *J. Am. Chem. Soc.* **1986,** *108*, 2388−2394.

30.   Jones, D. R.; Lindoy, L. F.; Sargeson, A. M., Hydrolysis of Phosphate Esters Bound to Cobalt(III). Kinetics and Mechanism of Intramolecular Attack of Hydroxide on Coordinated 4-Nitrophenyl Phosphate. *J. Am. Chem. Soc.* **1983,** *105*, 7327−7336.

31.   Kassai, M.; Teopipithaporn, R.; Grant, K. B., Hydrolysis of phosphatidylcholine by Cerium(IV) Releases Significant Amounts of Choline and Inorganic Phosphate at Lysosomal pH. *J. Inorg. Biochem.* **2011,** *105*, 215−223.

32.   Moss, R. A.; Morales-Rojas, H.; Vijayaraghavan, S.; Tian, J. Z., Metal-cation-mediated Hydrolysis of Phosphonoformate Diesters: Chemoselectivity and Catalysis. *J. Am. Chem. Soc.* **2004,** *126*, 10923−10936.

33.   Moss, R. A.; Ragunathan, K. G., Metal Cation Micelle Mediated Hydrolysis of Phosphonic Acid Esters. *Langmuir* **1999,** *15*, 107−110.

34.   Bracken, K.; Moss, R. A.; Ragunathan, K. G., Remarkably Rapid Cleavage of a Model Phosphodiester by Complexed Ceric Ions in Aqueous Micellar Solutions. *J. Am. Chem. Soc.* **1997,** *119*, 9323−9324.

35.   Geravand, E.; Farzaneh, F.; Gil-San-Millan, R.; Carmona, F. J.; Navarro, J. A. R., Mixed-Metal Cerium/Zirconium MOFs with Improved Nerve Agent Detoxification Properties. *Inorg. Chem.* **2020,** *59*, 16160−16167.

36.   Islamoglu, T.; Atilgan, A.; Moon, S. Y.; Peterson, G. W.; DeCoste, J. B.; Hall, M.; Hupp, J. T.; Farha, O. K., Cerium(IV) vs Zirconium(IV) Based Metal-Organic Frameworks for Detoxification of a Nerve Agent. *Chem. Mater.* **2017,** *29*, 2672−2675.

37.   Shigekawa, H.; Ishida, M.; Miyake, K.; Shioda, R.; Iijima, Y.; Imai, T.; Takahashi, H.; Sumaoka, J.; Komiyama, M., Extended X-ray Absorption Fine Structure Study on the Cerium(IV)-Induced DNA Hydrolysis: Implication to the Roles of 4f Orbitals in the Catalysis. *Appl. Phys. Lett.* **1999,** *74*, 460−462.

38.   Tabe, H.; Terashima, C.; Yamada, Y., Effect of Surface Acidity of Cyano-bridged Polynuclear Metal Complexes on the Catalytic Activity for the Hydrolysis of Organophosphates. *Catal. Sci. Technol.* **2018,** *8*, 4747−4756.

39.   Yamane, M.; Tabe, H.; Kawakami, M.; Tanaka, H.; Kawamoto, T.; Yamada, Y., Single Open Sites on Fe(II) Ions Stabilized by Coupled Metal Ions in CN-Deficient Prussian Blue

Analogues for High Catalytic Activity in the Hydrolysis of Organophosphates. *Inorg. Chem.* **2020,** *59*, 16000−16009.

40.   Aratani, Y.; Oyama, K.; Suenobu, T.; Yamada, Y.; Fukuzumi, S., Photocatalytic Hydroxylation of Benzene by Dioxygen to Phenol with a Cyano-Bridged Complex Containing Fe[II] and Ru[II] Incorporated in Mesoporous Silica-Alumina. *Inorg. Chem.* **2016,** *55*, 5780−5786.

41.   Kumar, K.; Chorazy, S.; Nakabayashi, K.; Sato, H.; Sieklucka, B.; Ohkoshi, S., TbCo and $Tb_{0.5}Dy_{0.5}Co$ Layered Cyanido-bridged Frameworks for Construction of Colorimetric and Ratiometric Luminescent Thermometers. *J. Mater. Chem. C* **2018,** *6*, 8372−8384.

42.   Chorazy, S.; Kumar, K.; Nakabayashi, K.; Sieklucka, B.; Ohkoshi, S., Fine Tuning of Multicolored Photoluminescence in Crystalline Magnetic Materials Constructed of Trimetallic $Eu_xTb_{1-x}[Co(CN)_6]$ Cyanido-Bridged Chains. *Inorg. Chem.* **2017,** *56*, 5239−5252.

43.   Song, X. J.; Zhang, Z. C.; Xu, Y. L.; Wang, J.; Zhou, H. B.; Song, Y., Assembling 1D Magnetic Chain Based on Octacyanotungstate(V) and $[Cu_2L_2Ln]$ Sub-building Units (Ln = Eu, Gd, Tb and Dy). *Dalton Trans.* **2013,** *42*, 9505−9512.

44.   Chelebaeva, E.; Long, J.; Larionova, J.; Ferreira, R. A. S.; Carlos, L. D.; Paz, F. A. A.; Gomes, J. B. R.; Trifonov, A.; Guerin, C.; Guari, Y., Bifunctional Mixed-Lanthanide Cyano-Bridged Coordination Polymers $Ln_{0.5}Ln'_{0.5}(H_2O)_5[W(CN)_8]$ (Ln/Ln′ = Eu^{3+}/Tb^{3+}, Eu^{3+}/Gd^{3+}, Tb^{3+}/Sm^{3+}). *Inorg. Chem.* **2012,** *51*, 9005−9016.

45.   Ma, S. L.; Ren, S., Novel Ladder-Like Structure Motif Assembled From Edge-Sharing Rhombus Squares Based on $[Mo^{iv}(CN)_8]^{4-}$ and Ln^{3+} (Ln = Tb and Eu) Ions as Building Blocks. *Synth. React. Inorg. Met. Org. Nano-Met. Chem.* **2010,** *40*, 299−305.

46.   Yamada, M.; Yonekura, S., Nanometric Metal-Organic Framework of Ln[Fe(CN)$_6$]: Morphological Analysis and Thermal Conversion Dynamics by Direct TEM Observation. *J. Phys. Chem. C* **2009,** *113*, 21531−21537.

47.   Kajiyama, S.; Mizuno, Y.; Okubo, M.; Kurono, R.; Nishimura, S.; Yamada, A., Phase Separation of a Hexacyanoferrate-Bridged Coordination Framework under Electrochemical Na-ion Insertion. *Inorg. Chem.* **2014,** *53*, 3141−3147.

48.   Bailey, W. E.; Williams, R. J.; Milligan, W. O., The Crystal Structure of LaFe(CN)$_6$·5H$_2$O. *Acta Crystallogr. B* **1973,** *29*, 1356−1368.

49.   Nakamoto, K., *Infrared and Raman Spectra of Inorganic and Coordination Compounds,* 6th Edition; John Wiley and Sons: New Jersey, **2009**.

50.   Zakharievapencheva, O.; Dementiev, V. A.; Forster, H., Far and Mid Infrared Spectra of MK(Fe(CN)$_6$)·4H$_2$O Complexes (M(III) = La, Nd, Sm, Eu, Gd, Tb, Dy, Ho, Yb): a Normal Coordinate Treatment. *J. Mol. Struct.* **1984,** *112*, 273−284.

51.   Zhou, X. J.; Duan, C. K.; Tanner, P. A., Luminescence and Crystal Field Analysis of Eu^{3+} in Eu[Co(CN)$_6$]·4H$_2$O. *J. Phys. Chem. Solids* **2007,** *68*, 1921−1925.

52.   Yamada, Y.; Yoneda, M.; Fukuzumi, S., A Robust One-Compartment Fuel Cell with a Polynuclear Cyanide Complex as a Cathode for Utilizing H$_2$O$_2$ as a Sustainable Fuel at Ambient Conditions. *Chem. Eur. J.* **2013,** *19*, 11733−11741.

53.   Li, B.; Raff, J.; Barkleit, A.; Bernhard, G.; Foerstendorf, H., Complexation of U(VI) with Highly Phosphorylated Protein, Phosvitin A Vibrational Spectroscopic Approach. *J. Inorg. Biochem.* **2010**, *104*, 718–725.

54.   Nguyen, N. K.; Leoni, M.; Maniglio, D.; Migliaresi, C., Hydroxyapatite Nanorods: Soft-template Synthesis, Characterization and Preliminary in vitro Tests, *J. Biomater. Appl.* **2013**, *28*, 49−61.

55.   Cho, H.; Cha, W., Rapid Hydrolysis of Organophosphates Induced by U(IV) Nanoparticles: A Kinetic and Mechanistic Study using Spectroscopic Analysis, *Colloids Interfaces* **2019**, *3*, 63.

56.   Olsson, R.; Giesler, R.; Loring, J. S.; Persson, P., Adsorption, Desorption, and Surface-Promoted Hydrolysis of Glucose-1-Phosphate in Aqueous Goethite (γ-FeOOH) Suspensions. *Langmuir* **2010**, *26*, 18760–18770.

57.   Doumic, L. I.; Salierno, G.; Ramos, C.; Haure, P. M.; Cassanello, M. C.; Ayude, M. A., "Soluble" vs. "Insoluble" Prussian Blue Based Catalysts: Influence on Fenton-type Treatment. *RSC Adv.* **2016**, *6*, 46625−46633.

58.   Pandey, P. C.; Panday, D., Tetrahydrofuran and Hydrogen Peroxide Mediated Conversion of Potassium Hexacyanoferrate into Prussian Blue Nanoparticles: Application to Hydrogen Peroxide Sensing. *Electrochim. Acta* **2016,** *190*, 758−765.

59.   Pandey, P. C.; Pandey, A. K., Novel Synthesis of Prussian Blue Nanoparticles and Nanocomposite Sol: Electro-analytical Application in Hydrogen Peroxide Sensing. *Electrochim. Acta* **2013,** *87*, 1−8.

60.   Scholz, F.; Schwudke, D.; Stösser, R.; Boháček, J., The interaction of Prussian Blue and Dissolved Hexacyanoferrate Ions with Goethite (α-FeOOH) Studied to Assess the Chemical Stability and Physical Mobility of Prussian Blue in Soils. *Ecotoxicol. Environ. Saf.* **2001**, *49*, 245−254.

61.   Dou, Y.; Yang, L.; Qin, L.; Dong, Y.; Zhou, Z.; Zhang, D., Efficient Hydrolytic Cleavage of Phosphodiester with a Lanthanide-based Metal-organic Framework. *J. Solid State Chem.* **2021**, *293*, 121820.

62.   Han, Q.; Zhang, L.; He, C. Niu, J. Duan, C., Metal−Organic Frameworks with Phosphotungstate Incorporated for Hydrolytic Cleavage of a DNA-Model Phosphodiester, *Inorg. Chem.* **2012**, *51*, 5118−5127.

63.   Dang, D.; Bai, Y.; He, C.; Wang, J.; Duan, C.; Niu, Structural and Catalytic Performance of POM-based Metal-organic Framework having Lanthanide Nanocage as a Secondary Building Block, *J. Inorg. Chem.* **2010**, *49*, 1280–1282.

64.   Yoshinari, N.; Meundaeng, N.; Tabe, H.; Yamada, Y.; Yamashita, S.; Nakazawa, Y.; Konno, T., Single-crystal-to-single-crystal Installation of $Ln_4(OH)_4$ Cubanes in an Anionic Metallosupramolecular Framework. *Angew. Chem. Int. Ed.* **2020**, *59*, 18048–18053.

65.   Oh, S. J.; Song, K. H.; Park, J. W., Catalytic Hydrolysis of Phosphate Monoesters by Lanthanide(III) Cryptate (2.2.1) Complexes. *J. Chem. Soc., Chem. Commun.* **1995**, 575–576.

66.   Dea, A.; Pradhanb, S. S.; Biswas, B., Coordinated Aqua Molecules Mediated Phosphoester Cleavage Activity of a Dimeric Gadolinium(III)-acetate. *J. Indian Chem. Soc.* **2017**, *94*, 1063–1071.

67.   Frey, S. T.; Hutchins, B. M.; Anderson, B. J.; Schreiber, T. K. Hagerman, M. E., Catalytic Hydrolysis of 4-Nitrophenyl Phosphate by Lanthanum(III)-Hectorite. *Langmuir* **2003**, *19*, 2188–2192.

Table of Contents

TOC graphic (8.25 cm × 3.84 cm)
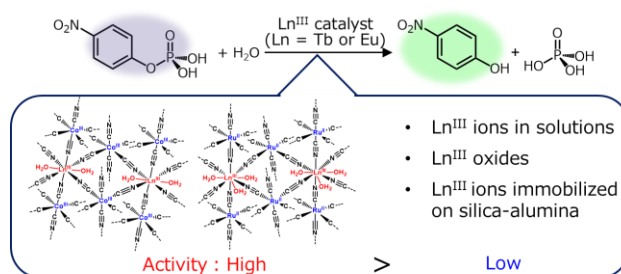
Synopsis

Heterogenization of trivalent lanthanoid (Ln^{III}) ion catalysts was carried out by preparation of lanthanoid oxides, immobilization of the Ln^{III} ions on a silica-alumina support, and syntheses of cyano-bridged coordination polymers containing Ln^{III} ions as the N-bound metal ions. The cyano-bridged coordination polymers exhibited the highest activity for hydrolysis of *p*-nitrophenyl phosphate due to the facile interaction between organophosphates and the limited inhibition by hydrolytic products as revealed by ex-situ IR spectroscopy.